Applicability of an iterative inversion algorithm to the diffraction patterns from inhomogeneously strained crystals

A. A. Minkevich,[1,*] T. Baumbach,[1] M. Gailhanou,[2] and O. Thomas[2]
[1]*Institute for Synchrotron Radiation, Forschungszentrum Karlsruhe, 76344 Eggenstein-Leopoldshafen, Germany*
[2]*IM2NP, UMR CNRS 6242, Université Paul Cézanne, 13397 Marseille Cedex 20, France*
(Received 15 August 2008; revised manuscript received 20 October 2008; published 25 November 2008)

The iterative phase retrieval algorithm and its applicability for the imaging of the deformation fields in crystals are investigated. For this reason the x-ray-diffracted data are simulated for the strained modeled crystal with different values of inhomogeneity of deformations. The influence of the constraints introduced by Minkevich *et al.* [Phys. Rev. B **76**, 104106 (2007)] to the iterative phase retrieval algorithm is shown for the reconstruction of highly inhomogeneous strain field.

DOI: 10.1103/PhysRevB.78.174110 PACS number(s): 61.05.cp, 62.20.−x, 42.30.Rx

I. INTRODUCTION

X-ray diffraction is well known for its capability of nondestructive determination of structures at the nanoscale. Being scattered by a particular object, experimentally detected x-ray intensity distribution contains detailed information about its internal structure. The problem is to extract the structural information from the measured x-ray intensities since phases are not experimentally available. In the case of artificial nanostructures, the model-dependent approaches are widely used (see, for example, Ref. 1). Making some assumptions about investigated structures, a model is built and scattered x-ray intensities' distributions are simulated. Trial-and-error or least-squares fitting procedures are then used to obtain the best agreement with experiments. However, the constructed model very often describes the sample only qualitatively because the investigated structures can be very complicated. For such cases, where there are specific troubles in implementing the fitting procedure, it is useful to have other approaches requiring as little as possible *a priori* data about investigated structures. The pioneering works concerning the direct imaging of the deformations in periodical crystalline structures from the diffraction patterns were published many years ago.[2,3] The theoretical studies of the advantages and limitations of the proposed method were published later.[4] The present work concentrates on the investigation of applicability of another modern technique called coherent diffractive imaging (CDI).[5,6] The direct-space electron density is retrieved with an iterative algorithm, first proposed by Gerchberg and Saxton[7] and further developed by Fienup.[8] The oversampled intensity information, satisfying the object sizes in direct space, for two-dimensional (2D) or higher-dimensional data in most cases corresponds to a unique set of phases in reciprocal space.[9] The possibility of directly determining the structure from a diffraction pattern alone was first mentioned by Sayre.[10] The noise and other experimental artifacts, of course, disturb this relation; however, it is supposed that notwithstanding this inaccuracy one solution exists. The nonuniqueness of "phase problem" for one-dimensional (1D) case can be also overcome by providing additional *a priori* information about an object as it was recently shown for some particular cases.[11,12] Presently many versions of the iterative algorithm were proposed as well as the comparisons of their convergence behavior properties.[13–15] The method is based on back-and-forth fast Fourier transforms (FTs) together with a set of constraints in both direct and reciprocal spaces. Since the FT is used, the approach is limited to the case where the interaction of matter with x rays is weak. This however covers a large number of experimental situations for which the x-ray extinction length is much greater than the analyzed object size. This approach has been very successful in yielding the density distribution of noncrystalline materials[5] and crystals.[16] In fact, the shape of diffracted intensity distributions around each Bragg reflection from nondeformed crystal is identical and centrosymmetric. Therefore, the direct-space density computed by inverse FT is real valued, representing the electron density of the corresponding crystal. The problems of nonconvergence for such a case can be often overcome by implementation of positivity constraint for the direct-space density. The presence of inhomogeneous strain breaks the centrosymmetry of Bragg peaks in reciprocal space (exceptions are only some special cases of centrosymmetric strain[17]). The direct-space data of such a crystal are already expressed by complex-valued numbers. The direct interpretation of the strained crystal density through complex-valued numbers is possible for quite small deformations, when we can only consider the shift of the crystal unit cell from its original position and neglect its internal deformations. Then, the amplitude corresponds to the amplitude of scattering potential (electron density) of the crystal and the phase is approximately given by the scalar product of the displacement $\vec{u}$ with the reciprocal Bragg vector $\vec{G}_{hkl}$.[18] The "direct-space" notation instead of conventional "real space" for the description of the object space is used in order to have no confusion between "real" and "complex." Only the amplitudes of the strained crystal density obtained by the inverse FT of its reciprocal space correspond to the real electron density. When the sample is described in the direct space by complex values, the convergence of the existing algorithms is often problematic and has hindered so far the general applicability of inversion to the diffraction of strained objects. It is important to note that for a complex-valued object, in the case where its imaginary part comes from absorption of x rays, usually it is possible to apply the positivity constraints to both the real and imaginary parts.[19] This was successfully

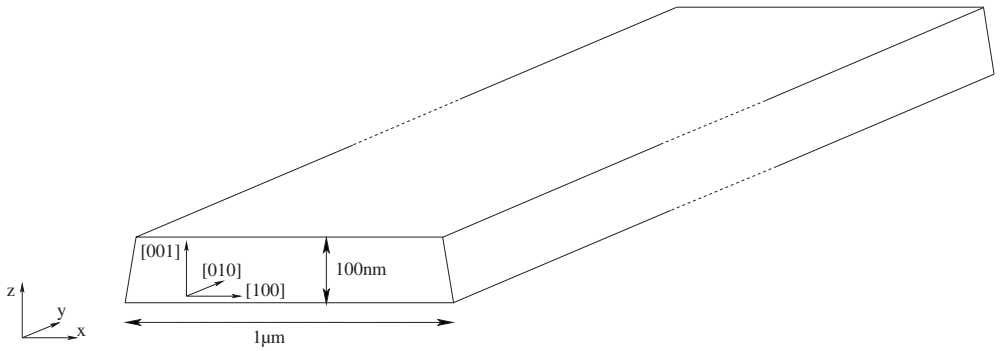

FIG. 1. Geometry of the modeled system.

illustrated in proceeding of experimental data.[20] The possibility of proceeding to the number of scattering measurements from overlapped object regions could also yield additional and sufficient information for the convergence of iterative algorithm.[21,22] Experimentally, implementation of the nonplanar curved beam illumination in small-angle scattering experiments was found positively influencing the convergence of the algorithm.[23] However, the precise stability (much higher than attained resolution in the direct space) of the sample is required in the last two cases. For some special shapes, especially when we have separated objects, the convergence may be achieved.[24] The first success concerning the case of a weakly strained nanocrystal has been recently obtained,[6] but inversion of a diffraction pattern from a very nonuniformly strained crystal remains an unsettled problem.

In a previous paper (see Ref. 25) the method for direct imaging of highly nonuniformly strained crystal was developed, which utilizes additional constraints to the spatial variation in displacement field (to the phases) together with density uniformity constraints (to the amplitudes). The method was successfully demonstrated with yielding a particular component of the deformation field distribution in 1-μm-wide silicon-on-insulator (SOI) line by inversion of the corresponding experimental diffraction pattern. The resulting displacement field was shown to be in excellent agreement with finite element modeling.[26] It was also shown that such values of deformations were only possible to reconstruct with the proposed additional constraints.[25] The inhomogeneous strain reaches the level of more than 10^{-3} for this case and is much larger than the deformations reconstructed in Ref. 6. The magnitude of inhomogeneous strain does not take into account the homogeneous strain component, which is not important for the direct reconstruction and only influences the Bragg-peak exact position. The purpose of this paper is to show the suitability of the proposed constraints for the reconstruction of the deformations with different values of inhomogeneity. This study is focused on numerical data. In Sec. II a modeled system based on the geometry of the system studied in Ref. 25 with different amplitudes of the displacement field is introduced. The basic features of the modified iterative algorithm can be found in Sec. III. Section IV contains the investigation of the convergence properties of the iterative algorithms for the inversion of the diffraction patterns simulated for our modeled system introduced in Sec. II.

II. MODELED SYSTEM

The modeled system is a perfect monocrystalline slab, infinite in the y direction and with a constant trapezoidal section on the (x,z) plane (Fig. 1). It is similar to the silicon-on-insulator system of reference,[25] and as in this latter case the monocrystal is silicon. The crystalline orientation of silicon with respect to the (x,y,z) frame is depicted in Fig. 1. The starting point for the calculations is the displacement field calculated using finite element analysis in Ref. 26, corresponding to an initial stress creating this displacement field, $\sigma=\sigma_0$. Then by variation in σ ($0.13\sigma_0$ and $0.013\sigma_0$), i.e., by a simple multiplication of the displacement field by a constant (0.13 and 0.013), we calculate several deformation fields and calculate the corresponding reciprocal-space maps (RSMs). The strain that appeared in our modeled system is fully 2D (plane strain) because of the system profile uniformity along the y direction.

We define the strain field inhomogeneity along chosen direction p (here x or z, for example) via the maximum variation range of the corresponding displacement field derivatives as

$$\Delta_p u_j^{\max} = \max\left[\frac{\partial u_j}{\partial p}\right] - \min\left[\frac{\partial u_j}{\partial p}\right]. \quad (1)$$

In Fig. 2 three 004 reciprocal-space maps are shown, corresponding to three different amplitudes of the displacement field ($x\|q_x\|$ silicon [100] direction; $z\|q_z\|$ silicon [001] direction). The relations between the variation ranges of the displacement field derivatives in Eq. (1) and different initial states of tension σ are placed in Table I. For the diffraction simulations the FT is used. In the case of the 004 Bragg reflection, the diffraction pattern contains only the information on the u_z component of the displacement field $\vec{u}$. From the differences between these RSMs, it is clearly seen the influence of strain on diffracted intensities. The σ values were chosen nonrandomly. The convergence properties of algorithm are different when taking the corresponding diffraction patterns. Additional constraints introduced in our previous work[25] are investigated here, namely, their importance for the reconstruction of high inhomogeneous strain. In addition in Fig. 3 the three corresponding diffraction patterns simulated near 206 reflection are shown. They also contain information on lateral component of deformation field u_x which has another space variation. For the $\sigma=0.013\sigma_0$ the

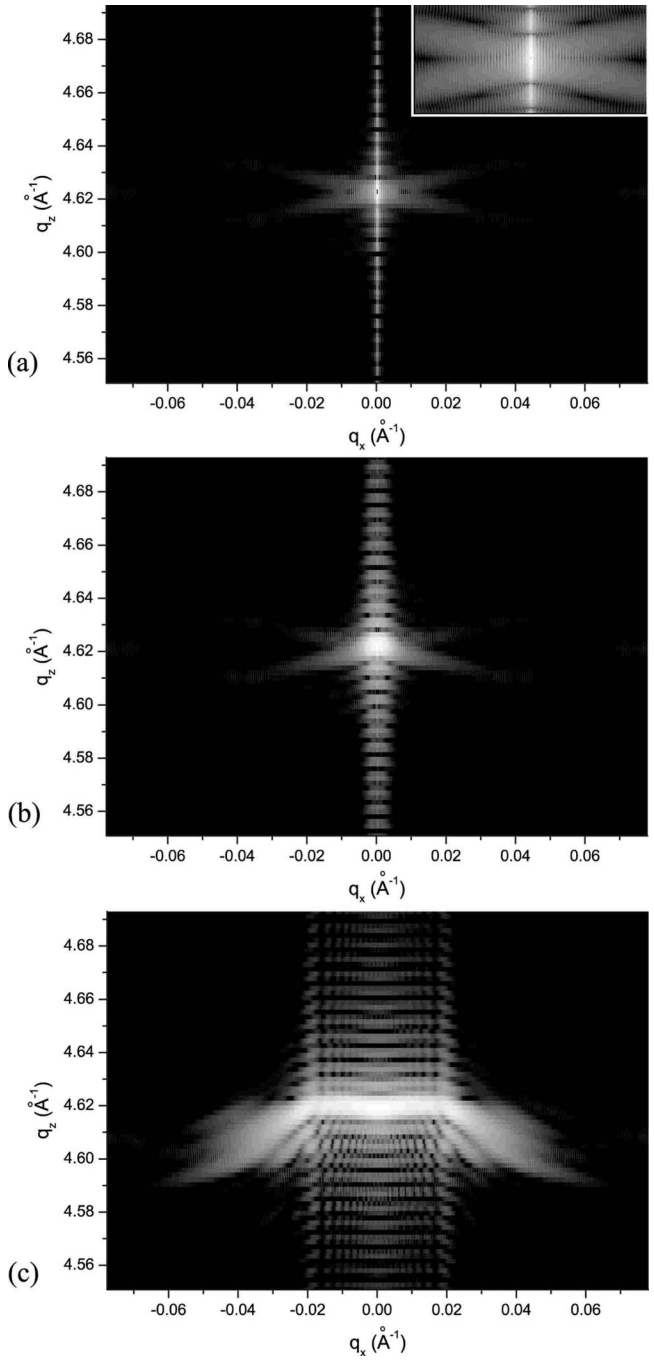

FIG. 2. Diffraction patterns simulated near 004 Bragg reflection from the silicon modeled system, corresponding to three different values of initial stress σ: (a) $0.013\sigma_0$, (b) $0.13\sigma_0$, and (c) σ_0. Inset of (a) shows the zoomed central part with intensity maximum of the RSM. The intensity scale is logarithmic.

diffraction patterns in both Figs. 2(a) and 3(a) are very similar to the one simulated from the unstrained crystal. The insets of these figures show the detailed shape of the diffracted intensity in the close vicinity of the reciprocal lattices. The inclined streaks with thickness modulations resulting from the scattering by trapezium-shaped system are not strongly disturbed by the impact of internal strain. This strain is very small and its influence on diffraction pattern is weak. The quality of experimental data and experimental artifacts

TABLE I. The relation between the initial states of tension σ and the variation ranges of the displacement derivatives [Eq. (1)] inside the silicon line.

σ	$\Delta_x u_x^{\max}$	$\Delta_z u_x^{\max}$	$\Delta_x u_z^{\max}$	$\Delta_z u_z^{\max}$
$0.013\sigma_0$	7×10^{-5}	4×10^{-4}	3×10^{-4}	9×10^{-5}
$0.13\sigma_0$	6.7×10^{-4}	4×10^{-3}	2.7×10^{-3}	9×10^{-4}
$1.0\sigma_0$	5×10^{-3}	3×10^{-2}	2×10^{-2}	7×10^{-3}

such as instrumental effects and integrated intensity in RSM, of course, negatively influence sensitivity to reconstruct and make the weak strain visible. The influence of different instrumental functions on ability to reconstruct the object by the iterative algorithm is another important topic and it was addressed recently.[27,28]

III. ADDITIONAL CONSTRAINTS OF RECONSTRUCTION ALGORITHM FOR STRAINED CRYSTAL DENSITY IMAGING

The reconstruction algorithm is based on iterative scheme which was originally developed many years ago by Fienup.[8] It includes error reduction (ER) and the hybrid input-output (HIO) iterative algorithms which are used together with the set of constraints in direct and reciprocal spaces. They iterate between both spaces and serve to recover the missing phases and consequently the direct-space object. At each algorithm iteration k, the difference between the calculated intensities and the experimental ones is expressed as

$$E_k^2 = \frac{\sum_{i=1}^{N} (|F_i^{\text{calc}}| - \sqrt{I_i^{\text{meas}}})^2}{\sum_{i=1}^{N} I_i^{\text{meas}}}, \tag{2}$$

where $|F_i^{\text{calc}}|$ is the magnitude of the calculated amplitude and I_i^{meas} is the measured intensity of point i in the RSM. The weakness of this approach is that it is valid only for the reconstruction of a real positive function. The possible stagnations which can happen in this case can be often overcome by implementation of the direct-space constraint that the result must be real and non-negative. In the case of a strained crystal, its direct-space density is not real and reconstruction is much more complicated. The success of complex-valued object reconstruction using only standard support constraint was reached only for particular cases, namely, for special object shapes[24] or sufficiently weakly strained Pb nanocrystal.[6] In many practical situations the object shapes do not satisfy the conditions denoted by Fienup,[24] namely, the shapes are convex and have many symmetric features. The spatial distribution and inhomogeneity of deformation field in crystal are also significant for convergence process. In general, as it was shown, for example, in the particular case of highly inhomogeneously strained silicon-on-insulator line, the standard support constraint cannot provide reliable convergence of iterative algorithm.[25] Consequently, in Ref.

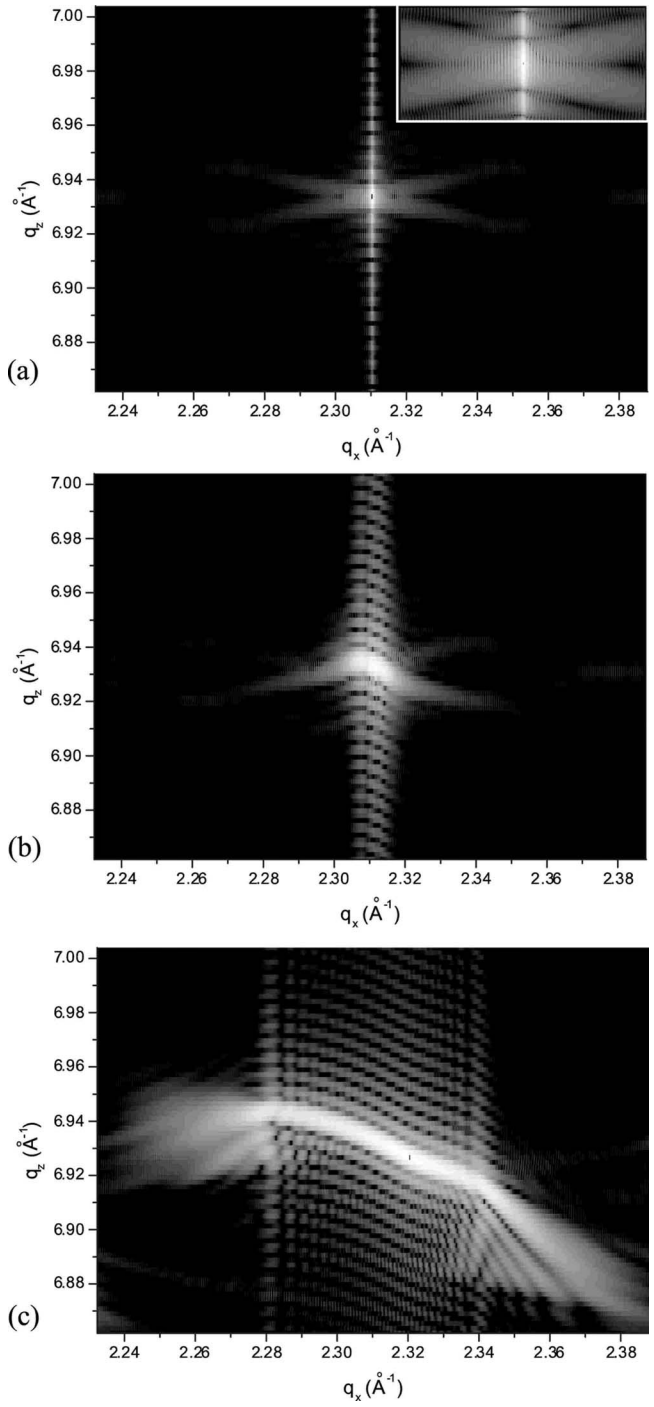

FIG. 3. Diffraction patterns simulated near 206 Bragg reflection from the silicon modeled system, corresponding to three different values of initial stress σ: (a) $0.013\sigma_0$, (b) $0.13\sigma_0$, (c) and σ_0. Inset of (a) shows the zoomed central part with intensity maximum of the RSM. The intensity scale is logarithmic.

25 in addition to the standard support constraint, two basic constraints were introduced and added to the iterative scheme. They were developed under the assumption of 2D plane strain and chemically homogeneous crystal; however, a generalization to three-dimensional (3D) systems might be foreseen. For clearness of further discussions these constraints are listed below:

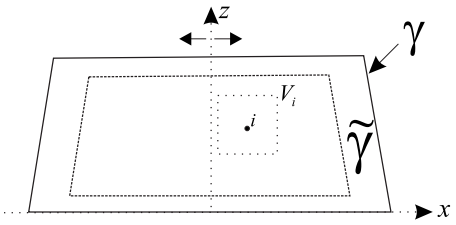

FIG. 4. Schematic sketch of the crystal cross section. V_i is the area around point i; $\tilde{\gamma}$ corresponds to a small region near support (γ) edges.

(I) The density, defined by direct-space amplitudes, must be uniform inside the support γ except for a small region near the support edges $\tilde{\gamma}$, where it decreases in the external direction from the support (Fig. 4):

$$a_{k+1}(i) = \begin{cases} a'_k(i), & |a'_k(i) - c_k(i)| < \epsilon \\ a_k(i) + \beta[c_k(i) - a'_k(i)], & |a'_k(i) - c_k(i)| > \epsilon, \end{cases}$$

$$c_k(i) = \begin{cases} 0, & i \notin \gamma \\ \dfrac{\sum_{\tilde{i} \in V_i} a_k(\tilde{i})}{N_{V_i}}, & i \in \gamma \setminus \tilde{\gamma} \\ a'_k(i), & i \in \tilde{\gamma}, \end{cases} \tag{3}$$

where $a_k(i)$ is the amplitude of point i of input at the k iteration; $a'_k(i)$ is the amplitude of point i of output at the k iteration, where the input $g_{k+1}(i) = a_{k+1}(i)e^{i\phi_{k+1}(i)}$ at the next iteration is taken from the output of the previous one by implementation of direct-space constraints (for definitions of input and output, see Ref. 8); β is a parameter taken in the [0.5,1.0] interval; ϵ is the parameter defining the threshold for applying the constraints in Eq. (3) to each individual point i in the direct-space map (DSM); V_i is the vicinity of point i, defining the set of neighboring points around point i; N_{V_i} is the number of points in the V_i; and $\tilde{\gamma}$ is the narrow edge of support, where the depth of this edge is defined by fittable parameters. The shape of V_i is not very important (disk, square, etc.). The number of points inside V_i should not, however, be too small. The amplitude profile inside the edge $\tilde{\gamma}$ is constructed automatically by the iterative algorithm.

(II) The second constraint is related to the maximum and minimum values that the components of the displacement derivatives $\frac{\partial u_j}{\partial p}$ can take. These maximum and minimum values limit the possible phase difference between neighboring points in the DSM:

$$\phi_{k+1}(i') - \phi_{k+1}(i) > \min\left[\frac{\partial u_j}{\partial p}\right]\Delta p G_{hkl},$$

$$\phi_{k+1}(i') - \phi_{k+1}(i) < \max\left[\frac{\partial u_j}{\partial p}\right]\Delta p G_{hkl}, \tag{4}$$

where $\max[\frac{\partial u_j}{\partial p}]\Delta p$ and $\min[\frac{\partial u_j}{\partial p}]\Delta p$ define the difference range in displacement component u_j between neighboring points i and i' $(i' > i)$ along p direction, and Δp is a step

along the p direction of the DSM defining the spatial resolution in this direction.

To make this constraint more efficient, it is necessary sometimes to define a minimum distance over which the displacement derivative $\frac{\partial u_j}{\partial p}$ sign is constant. These distances depend on the particular properties of the sample, such as shape, symmetry, and origin of strain, and they can be adjusted during an iterative process.

To implement these constraints in the iterative algorithm, the maximum and minimum values of the displacement derivatives have to be estimated. The exact values of the magnitudes $\max[\frac{\partial u_j}{\partial p}]$ and $\min[\frac{\partial u_j}{\partial p}]$ depend on the position of the Bragg peak, while their difference $\Delta_p u_j^{\max}$ does not. Within some uncertainty of exact Bragg-peak positioning, $\frac{\partial u_j}{\partial p}$ corresponds to the phases derivatives in RSM rather than actual displacement field derivatives from which $\frac{\partial u_j}{\partial p}$ deviate by some constant value. Their estimations could be approximately taken directly from the broadening of Bragg peak in RSM.[25] $G_{hkl}\max[\frac{\partial u_j}{\partial p}]$ and $G_{hkl}\min[\frac{\partial u_j}{\partial p}]$ will correspond, respectively, to the broadening left and right from the reciprocal-lattice point. For the particular case considered in the present paper, such estimations were sufficient for the reconstruction of the deformations. It means that the algorithm is not sensitive to the precise values of the maximum displacement derivatives. Alternatively instead of an estimation of the value of $\Delta_p u_j^{\max}$, a trial-and-error procedure with variation in the corresponding parameter can be easily performed.

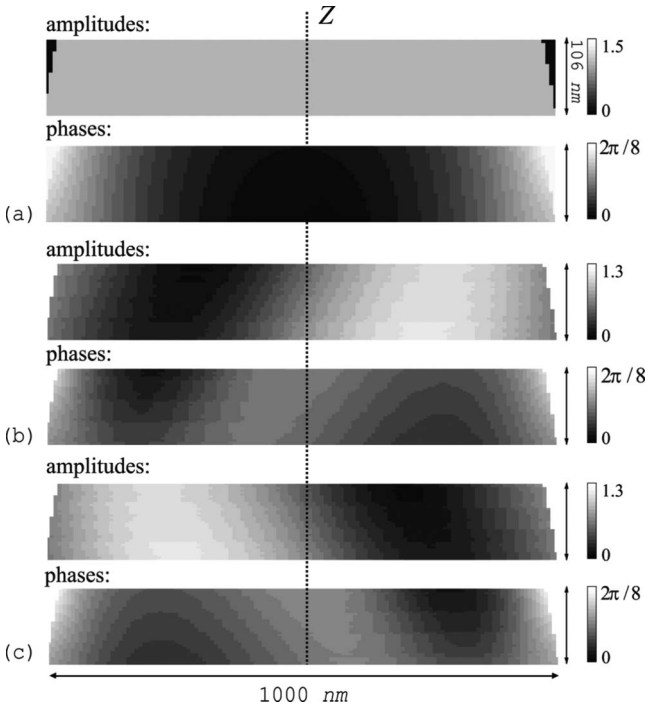

FIG. 5. The solution of the inverse problem for the RSM shown in Fig. 2(a) (for $\sigma=0.013\sigma_0$): (a) the correct solution; [(b) and (c)] two local minima L_1 and L_2, which are symmetric according to central axis Z. Only these two local minima were encountered for this case during convergence by ER+HIO. Amplitudes are in arbitrary units and phases are in radians.

IV. RESULTS OF RECONSTRUCTION AND DISCUSSION

The iterative phase retrieval algorithm was used to study the simulated RSMs for different values of initial state of tension σ resulting in different values of inhomogeneous strain (see Sec. II). Each time, the algorithm was applied with a new set of random phases in RSM. The standard support constraint which exactly corresponds to the shape of silicon line was used at the beginning. We start our investigation with inversion of the simulated diffracted data near symmetric 004 Bragg reflection, presented in Fig. 2. These data contain only information about the u_z component of the displacement field. For the value of $\sigma=0.013\sigma_0$ (for the related values of inhomogeneous strain components in silicon line, see Table I), there was no trouble in finding the correct solution using the standard procedure (without the additional constraints listed in Sec. III). Usually, it required several cycles; each cycle involved 50 iterations of HIO followed by 50 iterations of ER. The presence of ER in the iterative process is necessary; however, ER alone never provides the global convergence here. The HIO is used to escape and search for other local minima and together with ER it usually provides convergence. The corresponding solution of the inversion of the RSM corresponding to the initial state of tension $\sigma=0.013\sigma_0$ is plotted in Fig. 5(a). The phases in Fig. 5(a) directly correspond to the displacements in the silicon system via the relation $\phi=G_{004}u_z$. The probability of finding a correct solution, however, is not equal to unity. Together with the correct solution, two local minima $[L_1(x,z)$ and $L_2(x,z)]$ were discovered [see Figs. 5(b) and 5(c)]. From 100 program passes only 31 were successfully converging to the global minima, including convergence to the 180° rotated solution, because both object functions $f(x,y)$ and $f^*(-x,-y)$ have the same FT modulus. The probability of getting one of these solutions was approximately equal. The features of the rotated object were clearly recognized, however, as the shape of our support is not fully symmetric according to the 180° rotation; the stagnation appeared at the error metric level $E_k^2 \approx 10^{-4}$. In such a case, as it was suggested by Fienup,[29] it is simply necessary to restart the reconstruction from a completely new set of random phases. Despite the fact that only two local minima L_1 and L_2 were discovered during reconstruction, sometimes we had small stagnation near the global minima which was easily overcome by small perturbation, namely, by continuation of the convergence process with slightly changed parameter β (for example, $\beta=0.7$ was changed to 0.8). The exact object position determination in the space with respect to the 180° rotation, in other words top and bottom side determination, requires some *a priori* knowledge about the shape. For example, in the case of 1-μm-wide silicon-on-insulator system, we knew the direction of side inclination from the electron micrograph image.[25] The local minima defined by linear combination $t\rho(x,z)+(1-t)\rho^*(-x,-z)$ explained in Ref. 29 [$\rho(x,z)$ is the correct solution] was not encountered in our case. One of the reasons for this might be that our support is not fully symmetric according to 180° rotation. In our case the nature of the local minima is different. Their number increases with

increase in inhomogeneity of the displacement field. The inhomogeneity of the displacement field is characterized here by the maximum differences between corresponding displacement derivatives [Eq. (1)].

The presence and symmetry of the two local minima $L_1(x,z) \sim L_2(-x,z)$ ($x=0$ corresponds to the vertical axis Z) are provided by the symmetry of RSM according to $q_x=0$. Looking at the statistics of convergence results, the equal probability of getting one of these local minima is higher than the probability of getting a correct solution. After reaching one of them the algorithm stagnates near it on the error metric level $E_k^2 \approx 10^{-5}$. Further iterations produce no significant changes. The question is how to recognize the correct solution between all results of algorithm. Of course, for our pure simulated data which are exactly the square modulus of a FT of direct-space density, the error metric of correct solution goes down quickly to 0, in contrast with the case of local minima where it stagnates on some level ($\approx 10^{-5}$). But it is not the fact in the case of experimental data, which are only approximately described by FT. The importance of additional knowledge about an investigated object becomes comprehensible. For this easy case an implementation of the symmetry according to the Z axis or the density uniformity constraint immediately resolves the problem of the correct convergence.

The convergence situation changes when trying to invert the simulated x-ray data with increasing σ (or what is equivalent to the increasing inhomogeneous strain). The number of local minima increases. It is almost impossible in the case of the RSM corresponding to the $\sigma=0.013\sigma_0$ to find reliably the solution by the standard method using only support constraint. The number of local minima becomes too high, and the convergence to the right solution happens only as an occasion with very small probability. The results of algorithm depend on the starting set of random phases in RSM.

The presence of the local minima corresponds to ambiguous solutions because the error metric after reaching them becomes very small. This is especially the case for the experimental data where, because of the presence of noise, the difference between error metrics of correct and local minima solutions almost disappears. It means that for such complex-valued data, expressing inhomogeneously strained crystal, different combinations of amplitudes and phases in direct space can yield very similar FT amplitudes images. When the standard support constraint is used, once the algorithm has reached the local minima, it stagnates near it; i.e., further iterations do not produce any significant changes. In this case the zero-density region outside the support, arising from signal oversampling, cannot compensate for the unknown phases in the diffraction pattern because the values in this area become negligibly small. For the large convergence ambiguity, the number of local minima is very high, providing very small probability of finding correct solution for reasonable number of passes of iterative algorithm. The results of different algorithm starts are inconsistent. This reveals the instability of algorithm and impossibility of reconstructing the displacement field using only support constraint. The additional constraints become important for the convergence process.

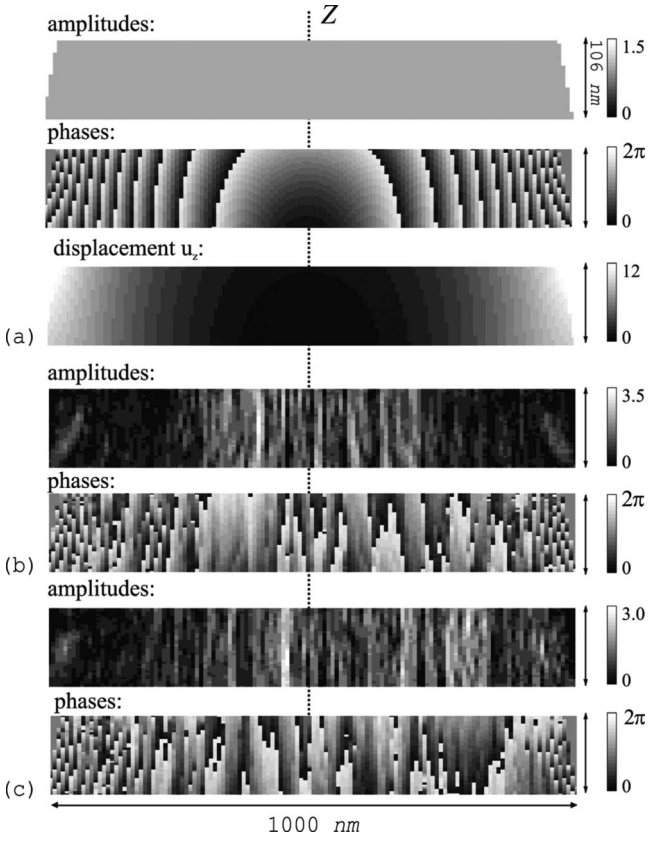

FIG. 6. Iterative inversion for the RSM shown in Fig. 2(c) (for $\sigma=\sigma_0$): (a) the correct solution; [(b) and (c)] typical results using conventional method. Amplitudes are in arbitrary units, displacements are in angstroms, and phases are in radians.

In the case of deformations corresponding to the initial residual stress $\sigma=0.13\sigma_0$, an implementation of density uniformity constraint is required and sufficient to solve the phase problem. The iterative algorithm was found to converge to the correct solution. The second constraint limiting the phase difference between neighboring points in DSM is redundant for such values of deformations in silicon system. A further increase in the inhomogeneity of the displacement field reveals the instability of algorithm even with density uniformity constraint. In this case the number of local minima is very large. The second constraint to the spatial phase variation coming from the maximum value of displacement derivative components becomes a key point in the reconstruction process. For the real values of deformations in the silicon system corresponding to the $\sigma=\sigma_0$, reliable reconstruction of u_z (z components of displacement field) requires addition of third complementary constraint to the sigh of displacement derivative. The third complementary constraint provides reliable convergence for imaging highly inhomogeneous strain in crystal. Without this constraint it is still possible to find a solution. However, the results are not very stable: the perturbations produced by constraints very often are not sufficient to find global minima and algorithm moves from one local minimum to another. The solution in this case [data from Fig. 2(c)] is shown in Fig. 6(a). For the large value of deformations presented here, the phases do not directly correspond to the displacement via the relation ϕ

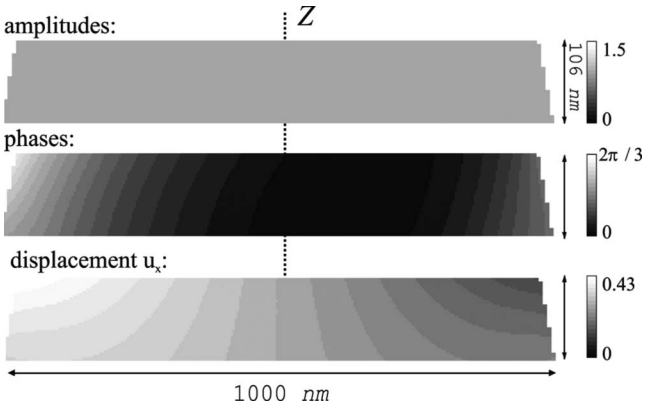

FIG. 7. Iterative inversion for the RSM shown in Fig. 3(a) (for $\sigma=0.013\sigma_0$): amplitudes, phases, and calculated u_x components of displacement field. For calculation of u_x, the phases of the present solution together with the u_z displacements retrieved from the corresponding 004 RSM were used. Amplitudes are in arbitrary units, phases are in radians, and displacements are in angstroms.

$=G_{004}u_z$. The displacement field is recalculated from the phase information taking into account the phase passing through 2π. For comparison two arbitrary local minima are shown after as well [Figs. 6(b) and 6(c)]. The number of local minima is incredibly high for this case.

Further investigation of convergence properties of algorithm was done by inversion of the simulated diffracted data near asymmetric 206 Bragg reflection (Fig. 3). These data contain information about both components of displacement field, u_z and u_x. In a way similar to the previous case of 004 reflection, three sets of data were simulated for the same values of initial state of tension σ.

During the inversion of the first set of data corresponding to the $\sigma=0.013\sigma_0$, similar to the 004 symmetric case two local minima together with correct solution were found. The local minima have features similar to the ones shown in Figs. 5(b) and 5(c) and resulted from the presence in reconstruction of the u_z component of displacement field. The problem of convergence is easily resolved by implementation of density uniformity constraint I [Eq. (3)]. The results of inversion are shown in Fig. 7. The further implementation of this procedure to the second set of data ($\sigma=0.13\sigma_0$) revealed the full instability of reconstruction using only standard support constraint, namely, a lot of local minima were observed. Both constraints I and II were required for reliable algorithm convergence. Constraint II was applied to the u_x component of displacement field. For this case, the phases in DSM at each point correspond to the $\phi=G_{006}u_z+G_{200}u_x$, and for u_x extraction the values u_z were taken from previous reconstruction for 004 RSM. The last RSM for $\sigma=\sigma_0$ [Fig. 3(c)] was also successfully processed with additional constraints as in the previous case (inversion results are shown in Fig. 8). It is important to point out that complementary constraint to the conservation of derivative sign of displacement field which was used for reliable inversion of data from Fig. 2(c) was not required for the present case. Moreover, the reconstruction was not sensitive to the precision of maximum value of displacement derivative used in constraint II. For example, for the displacement field in Fig. 8 the maximum value of $\frac{\partial u_x}{\partial x}$

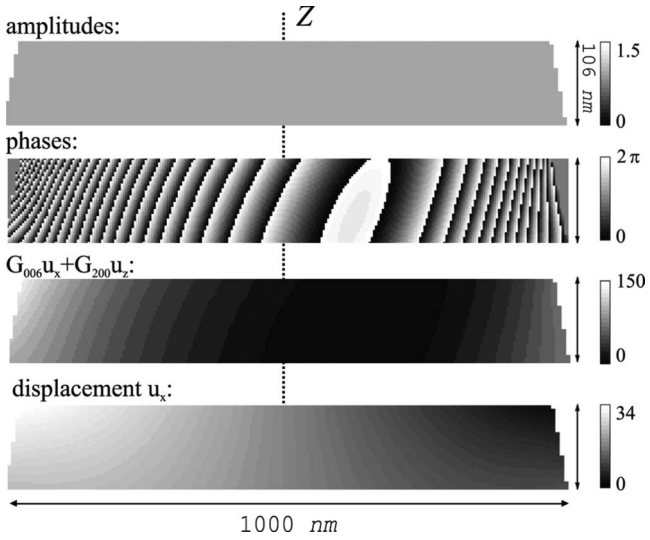

FIG. 8. Iterative inversion for the RSM shown in Fig. 3(c) (for $\sigma=\sigma_0$): amplitudes, phases, $(\vec{G}_{206}\vec{u})$ scalar products, and calculated (using retrieved beforehand u_z) u_x components of displacement field. Amplitudes are in arbitrary units, phases are in radians, and displacements are in angstroms.

$\approx 5\times 10^{-3}$. The successful reconstruction for this case was possible up to 2.5×10^{-2} maximum value for the derivative $\frac{\partial u_x}{\partial x}$ in constraint II. The further increase of this limit negatively influenced reconstruction and resulted in frequent stagnation of iterative process. As illustrated here, the exact estimation of the maximum displacement derivatives is not significant for these data and trial-and-error procedure can be easily performed incorporating several algorithm passes with different limits in constraint II. The estimations of the mentioned limits of the displacement derivatives are also possible.[25] For asymmetric map from Fig. 3(c) the maximum values of components of the projections of displacement $\vec{u}$ on $\vec{G}_{206}$ direction derivatives can be estimated. The large magnitude of the reciprocal-lattice vector $\vec{G}_{hkl}$ leads to larger phase variations in direct space and complicates the convergence of the algorithm.

It is necessary to point out that we also simulated the RSMs near 400 reflection for different values of σ_0 (not shown here) and tried to invert them. These RSMs contain information only about u_x component of displacement field. For the values $\sigma=0.013\sigma_0$ and $0.13\sigma_0$, the additional constraints I and II [Eqs. (3) and (4)] were unimportant. The solutions—u_x components of displacement fields—were found using only support constraint without any difficulties; no local minima were observed. Constraint I became important for reconstruction of u_x field corresponding to the $\sigma > 0.33\sigma_0$. To extract the deformations from 400 RSM corresponding to the $\sigma=\sigma_0$, both constraints I and II are required. The complementary constraint to the sign of displacement derivatives, which was used to invert 004 reflection RSM for the same stress value, was not useful for u_x reconstruction. We obtained reliable convergence without this complementary constraint.

In general, the importance of the additional constraints, of course, depends on the value as well as the spatial distribu-

tion of deformation field in crystal to be reconstructed. For some cases they are less important, or even not important at all.[6] For other cases as it was shown here they are highly required. For the values of deformations that appeared in real case of silicon system (see Table I for the $\sigma=\sigma_0$), reconstruction using only a support constraint is probably possible as an occasion. However, we never reached it producing hundreds of algorithm trials starting from random phases in RSM. There are some sets of phases in RSM which belong to some phase vicinity corresponding to the global minima (solution). Starting algorithm from RSM image with phases belonging to this vicinity occurs in global minima after several iterations. But what is the probability that random phases in RSM satisfy this condition and appertain to this vicinity? In this paper it is shown that the probability of getting the solution by standard phase retrieval technique decreases with increasing inhomogeneity of deformation field [Eq. (1)], which is equivalent to the size of this vicinity decreasing. For the highest deformations in silicon shown here, the probability that random phases in RSM occur in the vicinity, from which the solution can be directly reached without introduced additional constraints I and II, is incredibly small. In the case where the solution as an occasion is reached nevertheless, it is difficult to monitor it as the error metrics of usually found local minima are very small too.

Here, it is illustrated that the correct global solution is possible to find using model-independent approach, but with implementation of additional constraints. The cost of these constraints is not very high, as the algorithm is not sensitive to precise value of the maximum value of displacement derivative which can be approximately estimated from the Bragg-peak broadening.

V. CONCLUSION

The iterative phase retrieval algorithm was applied to retrieve the displacement field with different values of inhomogeneity inside modeled silicon slab. It is shown that the displacement field in a strained crystal can be retrieved from its x-ray-diffraction pattern alone. However, the required convergence conditions depend on the value of inhomogeneity of displacement field in crystal. The comparison of convergence behaviors of this algorithm was illustrated for reconstruction of different strain fields. The standard support constraint provides satisfactory convergence only for weakly inhomogeneous displacement field. The increased inhomogeneity of displacement field, depending on maximum difference of corresponding displacement derivatives [Eq. (1)], causes the increase in ambiguity in reconstruction process together with decrease in probability of finding the correct solution. The developed constraints to spatial displacement variations and density uniformity serve to remove this ambiguity in the reconstruction process. Their significance is shown for retrieving of gradually increasing deformation field. The present research contributes to the investigation of the advantages and limitations of the modern and promising CDI technique for the imaging of deformations in microcrystals with high spatial resolution.

*andrey.minkevich@iss.fzk.de

[1] T. Baumbach, D. Luebbert, and M. Gailhanou, J. Appl. Phys. **87**, 3744 (2000).
[2] V. V. Aristov, T. E. Gureyev, A. Y. Nikulin, P. V. Petrashen, and A. A. Snigirev, Semicond. Sci. Technol. **7**, 1109 (1992).
[3] A. Y. Nikulin, T. E. Gureyev, A. W. Stevenson, S. W. Wilkins, H. Hashizume, and D. Cookson, J. Appl. Crystallogr. **28**, 803 (1995).
[4] A. Y. Nikulin, Phys. Rev. B **57**, 11178 (1998).
[5] J. Miao, P. Charalambous, J. Kirz, and D. Sayre, Nature (London) **400**, 342 (1999).
[6] M. A. Pfeifer, G. J. Williams, I. A. Vartanyants, R. Harder, and I. K. Robinson, Nature (London) **442**, 63 (2006).
[7] R. W. Gerchberg and W. O. Saxton, Optik (Stuttgart) **35**, 237 (1972).
[8] J. R. Fienup, Appl. Opt. **21**, 2758 (1982).
[9] R. H. T. Bates, Optik (Stuttgart) **61**, 247 (1982).
[10] D. Sayre, Acta Crystallogr. **5**, 843 (1952).
[11] I. Vartanyants, C. Ern, W. Donner, H. Dosch, and W. Caliebe, Appl. Phys. Lett. **77**, 3929 (2000).
[12] O. Bunk, A. Diaz, F. Pfeiffer, C. David, B. Schmitt, D. K. Satapathy, and J. F. van der Veen, Acta Crystallogr., Sect. A: Found. Crystallogr. **63**, 306 (2007).
[13] V. Elser, J. Opt. Soc. Am. A **20**, 40 (2003).
[14] H. H. Bauschke, P. L. Combettes, and D. R. Luke, J. Opt. Soc. Am. A **19**, 1334 (2002).
[15] S. Marchesini, Rev. Sci. Instrum. **78**, 011301 (2007).
[16] G. J. Williams, M. A. Pfeifer, I. A. Vartanyants, and I. K. Robinson, Phys. Rev. B **73**, 094112 (2006).
[17] S. Labat, V. Chamard, and O. Thomas, Thin Solid Films **515**, 5557 (2007).
[18] S. Takagi, J. Phys. Soc. Jpn. **26**, 1239 (1969).
[19] J. Miao, D. Sayre, and H. N. Chapman, J. Opt. Soc. Am. A **15**, 1662 (1998).
[20] R. A. Dilanian and A. Y. Nikulin, Appl. Phys. Lett. **87**, 161904 (2005).
[21] J. M. Rodenburg, A. C. Hurst, A. G. Cullis, B. R. Dobson, F. Pfeiffer, O. Bunk, C. David, K. Jefimovs, and I. Johnson, Phys. Rev. Lett. **98**, 034801 (2007).
[22] P. Thibault, M. Dierolf, A. Menzel, O. Bunk, C. David, and F. Pfeiffer, Science **321**, 379 (2008).
[23] G. J. Williams, H. M. Quiney, B. B. Dhal, C. Q. Tran, K. A. Nugent, A. G. Peele, D. Paterson, and M. D. de Jonge, Phys. Rev. Lett. **97**, 025506 (2006).
[24] J. R. Fienup, J. Opt. Soc. Am. A **4**, 118 (1987).
[25] A. A. Minkevich, M. Gailhanou, J.-S. Micha, B. Charlet, V. Chamard, and O. Thomas, Phys. Rev. B **76**, 104106 (2007).
[26] M. Gailhanou, A. Loubens, J.-S. Micha, B. Charlet, A. A. Minkevich, R. Fortunier, and O. Thomas, Appl. Phys. Lett. **90**, 111914 (2007).
[27] I. A. Vartanyants and I. K. Robinson, J. Phys.: Condens. Matter **13**, 10593 (2001).
[28] G. J. Williams, H. M. Quiney, A. G. Peele, and K. A. Nugent, Phys. Rev. B **75**, 104102 (2007).
[29] J. R. Fienup and C. C. Wackerman, J. Opt. Soc. Am. A **3**, 1897 (1986).